 CMES, vol.68, no.2, pp.117-149, 2010

MLPG analysis of Nonlinear Heat Conduction in Irregular Domains

Harishchandra Thakur[1], **K. M. Singh**[2] **and P. K. Sahoo**[3]

Abstract: MLPG method is a meshfree method which removes the need of meshing of computational domain at any stage of numerical analysis. Current article extends MLPG method to nonlinear heat conduction in irregular domains including the problem of solid-liquid phase change. Moving least square (MLS) scheme is used to interpolate the trial function and a fourth order spline function is used as the test function. Method of direct interpolation is used to enforce essential boundary conditions. Nonlinearities in the problems are handled with an iterative predictor-corrector method. Time integration is performed using θ-method. MLPG method has also been extended to non-homogeneous heat conduction. MLPG results are found to be in a good agreement with available exact solution/ FEM results.

Keywords: MLPG, nonlinear conduction, phase change, MLS approximation

1 Introduction

Most of the engineering problems by their true nature are nonlinear. But, due to known ease in analysis, systems with nonlinearity are often reduced to linear problems. In many instances, assumptions of linearity may lead to reasonable idealization of the behavior of the system. However, this may result in serious error in some cases. Designing high performance and efficient components for aerospace, defense and nuclear industries and establishing causes of system failure are few cases where only nonlinear analysis can provide accurate solutions. Geometrical nonlinearity, nonlinearity due to varying material properties and nonlinearity due

[1] Department of Mechanical Engineering, College of Engineering Roorkee, Roorkee, Roorkee-247667, India. E-mail: harishcthakur2k1@rediffmail.com

[2] Corresponding author. Department of Mechanical and Industrial Engineering, Indian Institute of Technology Roorkee, Roorkee-247667, India. E-mail: singhfme@gmail.com, singhfme@iitr.ernet.in

[3] Department of Mechanical and Industrial Engineering, Indian Institute of Technology Roorkee, Roorkee-247667, India. E-mail: sahoofme@iitr.ernet.in

to boundary conditions are the main reasons which create nonlinearity in the real engineering problems.

A number of numerical techniques have been applied to solve nonlinear conduction problems in the literature. FEM based formulations can be seen in Trujillo and Busby (1977), Bathe and Koshgoftaar (1979), Ling and Surana (1994) and Yang (1999) where convection and radiation boundary conditions or variable thermal properties of the material have been taken as reason of nonlinearity in the problem. Chan (1993) and Liao (1997) have applied boundary element method (BEM) to solve the nonlinear heat transfer problems. Meshfree methods have also been extended to solve many nonlinear heat transfer problems. Singh, Singh and Prakash (2006, 2007) have successfully extended element free Galerkin (EFG) method to solve nonlinear heat conduction problems with variable thermal conductivity of the material.

FEM and BEM are conventional mesh based method. EFG is a popular meshfree method but a background mesh is still required to perform integration of the weak form of the governing differential equation. In contrast, meshless local Petrov-Galerkin (MLPG) method does not need meshing of computational domain at any stage of analysis [Atluri and Zhu (1998a, 1998b); Atluri and Zhu (2000); Atluri and Shen (2002b)]. MLPG method, due to its vast potential of formulation has been extended successfully in the area of solid mechanics [Atluri and Zhu (2000); Atluri and Shen (2002b)]. MLPG method has been also applied to different types of heat transfer problems. Sladek, Sladek and Atluri (2004) applied MLPG method to solve heat conduction problem in anisotropic medium. Quin and Batra (2005) applied MLPG method to compute three-dimensional transient heat-conduction problem. Wu and Tao (2008) applied MLPG mehod to solve steady state conduction problems in irregular domain and compared the results obtained by finite volume method. Sterk and Trobec (2008) applied MLPG method to solve transient heat conduction problem in regular and irregular domain and compared the results with results of FEM. They also obtained the optimum parametric values used in MLPG method. Thakur, Singh and Sahoo (2009) have applied MLPG method to nonlinear heat conduction in regular domains. Current article is an extension of MLPG method to the problems of nonlinear heat conduction in irregular domains, including problems involving solid-liquid phase change.

Moving least square (MLS) approximation is a popular meshfree technique to approximate the trial function. This technique has been used in the current article. A fourth order spline weight function is used in the MLS approximation. Following sections show MLPG formulation of the nonlinear heat conduction problem followed by detailed results and discussion for different test problems.

2 Governing Differential Equation

Consider heat conduction in an isotropic domain Ω. Thermo-physical properties of the material vary with temperature. The governing partial differential equation for the problem is given by

$$\nabla \cdot [k(T)\nabla T] + Q_g = \rho(T)c(T)\dot{T} \tag{1}$$

Initial and boundary conditions are given as follows:
Initial condition

$$T(x,0) = T_o \text{ on } \bar{\Omega} \tag{2}$$

Boundary conditions

$$\begin{cases} T = \bar{T} & \text{on } \Gamma_1 \\ k(T)\frac{\partial T}{\partial n} = \bar{q} & \text{on } \Gamma_2 \\ k(T)\frac{\partial T}{\partial n} = h(T_a - T) & \text{on } \Gamma_3 \end{cases} \tag{3}$$

where $\Gamma = \Gamma_1 \cup \Gamma_2 \cup \Gamma_3$ is the boundary of global domain Ω, $\bar{T}$ is the specified temperature on essential boundary, $\bar{q}$ is the given flux at the natural boundary, $\mathbf{n}$ is the outward unit normal to the boundary, h is convective heat transfer coefficient and T_a is ambient temperature.

2.1 Phase Change Problems

For the solution of the problem involving solidification or freezing, two equations of the form (1), one in solid and one in liquid, are solved along with conditions on the domain boundaries. The following equations are required to be satisfied additionally on the interface of the two phases for $t > 0$ and at $\mathbf{x} = s(t)$:

$$T_s = T_l = T_f \tag{4}$$

$$k_l \left(\frac{\partial T}{\partial n}\right)|_{\mathbf{x}=s(t)} + k_s \left(\frac{\partial T}{\partial n}\right)|_{\mathbf{x}=s(t)} = \rho L \frac{\partial s}{\partial t} \tag{5}$$

where the subscripts l and s represent liquid and solid phases respectively, L is the latent heat of the material, T_f is the freezing temperature and $s(t)$ is the solidification front at instant of time t. Equation (5) accounts for the liberation of latent heat at the solidification front. As the location of the interface is not known *a priori*, hence, Eq. (1) becomes a nonlinear problem. Available exact solutions are very few and they are restricted to simple geometries with simple boundary conditions.

The apparent capacity method, which removes the need of tracking interface at the run time, is employed here to solve the solidification problems in irregular domains. In this method, interface location is derived afterwards from the calculated temperature field. This is possible because the phase front conditions are implicitly accounted for in the definition of the enthalpy. Enthalpy is defined as integral of heat capacity with respect to temperature and is written as

$$H = \int_{T_{ref}}^{T} \rho(T)c(T)dT \tag{6}$$

Thus,

$$\frac{dH}{dT} = \rho(T)c(T) \tag{7}$$

Putting Eq. (7) in Eq. (1) results in the following equation:

$$\nabla \cdot [k(T)\nabla T] + Q_g = \frac{dH}{dT}\dot{T} \tag{8}$$

Now, instead of solving Eq. (1) in liquid and solid separately, only Eq. (8) is solved in entire domain for phase change problems.

3 Numerical Method

The MLPG method is a meshfree method which has been developed by Atluri and his co-workers [Atluri and Zhu (1998a, 1998b); Atluri and Zhu (2000); Atluri and Shen (2002b)]. The basic concept of this method comes from the idea of local weak form of the governing differential equations. Trial functions in the analysis are generated using a set of nodes locally surrounding the point of interest and integration is performed in a conveniently chosen local domain. Due to Petrov-Galerkin formulation, test function is selected from different functional space. This leads to various possible formulations of MLPG method. This method is also claimed to be truly meshfree method as it avoids meshing of entire computational domain at any stage of analysis.

A variety of local interpolation schemes are available in literature. The moving least square (MLS) scheme [Lancaster and Salkauskas (1981)], Shepard functions [Shepard (1968)], partition of unity methods [Babuska and Melenk (1997)], reproducing kernel particle methods [Liu, Chen, Chang and Belytschko (1996)] and radial basis functions [Wendland (1995)] are few among them. The moving least squares (MLS) method is generally considered to be one of the best schemes to interpolate data with a reasonable accuracy. A brief idea of MLS scheme is presented in following section.

3.1 Moving Least Squares (MLS) Approximation

Consider an arbitrary point of interest **x** located in the problem domain. The moving least squares approximant $u^h(\mathbf{x})$ of $u(\mathbf{x})$ is given as

$$u^h(\mathbf{x}) = \sum_{j=1}^{m} p_j(\mathbf{x}) a_j(\mathbf{x}) \equiv \mathbf{p}^T(\mathbf{x})\mathbf{a}(\mathbf{x}) \tag{9}$$

where $\mathbf{p}^T(\mathbf{x}) = [p_1(\mathbf{x}), p_2(\mathbf{x}), \ldots\ldots, p_m(\mathbf{x})]$ is a complete monomial basis and m is the number of terms in the basis. For example, in 2-D space the basis can be chosen as

$$\begin{aligned} &\text{Linear basis: } \mathbf{p}^T(\mathbf{x}) = \{1,\ x_1,\ x_2\},\ m\ =\ 3 \\ &\text{Quadratic basis: } \mathbf{p}^T(\mathbf{x}) = \{1,\ x_1, x_2, x_1^2,\ x_1x_2,\ x_2^2\},\ m\ =\ 6 \end{aligned} \tag{10}$$

The coefficient vector **a(x)** is determined by minimizing a weighted discrete L_2 norm defined as

$$J = \sum_{i=1}^{n} w(\mathbf{x}, \mathbf{x}_i)[u^h(\mathbf{x}) - u(\mathbf{x}_i)]^2 = \sum_{i=1}^{n} w(\mathbf{x}, \mathbf{x}_i)[\mathbf{p^T}(\mathbf{x_i})\mathbf{a}(\mathbf{x}) - u(\mathbf{x}_i)]^2 \tag{11}$$

where $w(\mathbf{x}, \mathbf{x}_i)$ is a weight function and is explained in the next section. $u(\mathbf{x}_i) = u_i$ is the nodal parameter of the field variable at node $\mathbf{x}_i$ and n is the number of nodes in the support domain of **x** for which the weight function, $w(x, x_i) \neq 0$. The stationarity of J in Eq. (11) with respect to **a(x)** results in the following linear system:

$$\mathbf{A}(\mathbf{x})\mathbf{a}(\mathbf{x}) = \mathbf{B}(\mathbf{x})\mathbf{u} \tag{12}$$

The above equation can be written as

$$\mathbf{a}(\mathbf{x}) = \mathbf{A}^{-1}(\mathbf{x})\mathbf{B}(\mathbf{x})\mathbf{u} \tag{13}$$

where matrices **A, B** and **u** are defined as

$$\mathbf{A}(\mathbf{x}) = \sum_{i=1}^{n} w(\mathbf{x}, \mathbf{x}_i)\mathbf{p}(\mathbf{x}_i)\mathbf{p^T}(\mathbf{x}_i) \tag{14}$$

$$\mathbf{B}(\mathbf{x}) = [w(\mathbf{x}, \mathbf{x}_1)\mathbf{p}(\mathbf{x}_1), w(\mathbf{x}, \mathbf{x}_2)\mathbf{p}(\mathbf{x}_2), \ldots\ldots, w(\mathbf{x}, \mathbf{x}_n)\mathbf{p}(\mathbf{x}_n)] \tag{15}$$

$$\mathbf{u}^{=}[u_1, u_2, \ldots u_n]^T \tag{16}$$

System of equations (13) for **a(x)** is solvable if **A** is a nonsingular matrix. The requirement of the nonsingularity of **A** is$n > m$. Hence, the support domain of

point **x** must cover number of nodes which is higher than the number of terms in the monomial basis.

Substituting Eq. (13) in Eq. (9), the MLS approximant is obtained as

$$u^h(\mathbf{x}) = \sum_{i=1}^{n} \Phi_i u_i = \mathbf{\Phi}(\mathbf{x})\mathbf{u} \tag{17}$$

where meshless shape function $\Phi_i(\mathbf{x})$ is defined as

$$\Phi_i(\mathbf{x}) = \sum_{j=1}^{m} p_j(\mathbf{x}) \left(\mathbf{A}^{-1}(\mathbf{x})\mathbf{B}(\mathbf{x})\right)_{ji} \tag{18}$$

The partial derivatives of $\Phi_i(\mathbf{x})$ are obtained as

$$\Phi_{i,k}(\mathbf{x}) = \sum_{j=1}^{m} [p_{j,k}(\mathbf{A}^{-1}\mathbf{B})_{ji} + p_j(\mathbf{A}^{-1}\mathbf{B}_{,k} + \mathbf{A}^{-1}_{,k}\mathbf{B})_{ji}] \tag{19}$$

in which $()_{,k}$ denotes $\partial()/\partial x_k$ and $\mathbf{A}^{-1}_{,k}$ represents the derivative of the inverse of **A** given by

$$\mathbf{A}^{-1}_{,k} = -\mathbf{A}^{-1}\mathbf{A}_{,k}\mathbf{A}^{-1} \tag{20}$$

3.2 Weight Function

The choice of weight function affects the resulting approximation $u^h(\mathbf{x})$. The smoothness of the meshless shape function is governed by smoothness of the weight function. Therefore, selection of an appropriate weight function is essential. The weight function $w(\mathbf{x}, \mathbf{x}_i)$ is non-zero over a small domain in the neighborhood of node $\mathbf{x}_i$ called the domain of influence. The fourth order spline weight function is used which is given by

$$w(\mathbf{x}, \mathbf{x_i}) = \begin{cases} 1 - 6d^2 + 8d^3 - 3d^4 & \text{if } 0 \le d \le 1 \\ 0 & \text{if } d > 1 \end{cases} \tag{21}$$

In the preceding equation, $d = d_i/r$, $d_i = \|\mathbf{x} - \mathbf{x}_i\|$ (i.e. the Euclidean distance from node $\mathbf{x}_i$ to point **x)**, and r is the radius of support domain in which weight function is non-zero.

3.3 MLPG Formulation

In MLPG formulation, integration is performed over a local domain to establish discrete system of equations. The local quadrature domain Ω_Q is chosen conveniently. In the current formulation, a circle centered at point $\mathbf{x}$ is selected as the local domain.

A general weak form of Eq. (1) can be obtained from the weighted residual statement

$$\int_{\Omega_Q} \left\{ \nabla \cdot [k(T)\nabla T] + Q_g - \rho(T)c(T)\dot{T} \right\} v \, \mathrm{d}\Omega = 0 \tag{22}$$

where v is the test function. Using divergence theorem, Eq. (22) yields the desired weak form given by

$$\int_{\partial\Omega_Q} k(T)T_{,i}n_i v \, \mathrm{d}\Gamma - \int_{\Omega_Q} \left[k(T)T_{,i}v_{,i} - Q_g v + \rho(T)c(T)\dot{T}v \right] \mathrm{d}\Omega = 0 \tag{23}$$

where $\partial\Omega_Q$ is the boundary of the local domain Ω_Q.

Petrov-Galerkin formulation enables MLPG method to choose test and trial functions independently and this makes possible to perform integration in a local quadrature domain. The weight function of the MLS approximation is used as the test function (formulation is popularly known as MLPG1) in the present work. It is chosen to vanish at the boundary of the local domain. Hence, evaluation of the boundary integral term in Eq. (23) is not required for a local domain entirely inside the problem domain Ω_s. The method of direct interpolation [Liu (2003)] is used to impose essential boundary conditions.

This discretization procedure leads to an ordinary differential equation for each node. Collection of ordinary differential equations for the internal nodes combined with boundary nodes results in the system of ODEs given by

$$\mathbf{C}(\mathbf{T})\dot{\mathbf{T}} + \mathbf{K}(\mathbf{T})\mathbf{T} = \mathbf{F} \tag{24}$$

where $\mathbf{T}$ is the vector of unknown nodal temperatures. The damping matrix $\mathbf{C}$, the stiffness matrix $\mathbf{K}$ and the load vector $\mathbf{F}$ are as follows:

$$C_{ij} = \begin{cases} \int_{\Omega_Q} \rho(T)c(T)v(\mathbf{x},\mathbf{x_i})\Phi_j(\mathbf{x})\,\mathrm{d}\Omega & \mathbf{x}_i \notin \Gamma \\ 0 & \text{otherwise} \end{cases} \tag{25}$$

$$F_i = \begin{cases} \bar{T} & \mathbf{x}_i \in \Gamma_1 \\ \int_{\Gamma_{2Q}} v_i \bar{q}\,\mathrm{d}\Gamma + \int_{\Gamma_{3Q}} v_i h T_a \mathrm{d}\Gamma + \int_{\Omega_Q} Q_g v_i \mathrm{d}\Omega & \text{otherwise} \end{cases} \tag{26}$$

where $\Gamma_{1Q} = \Gamma_1 \cap \partial\Omega_Q$, $\Gamma_{2Q} = \Gamma_2 \cap \partial\Omega_Q$ and $\Gamma_{3Q} = \Gamma_3 \cap \partial\Omega_Q$.
For the process of phase change, only damping matrix will change which can be expressed as

$$C_{ij} = \begin{cases} \int_{\Omega_Q} \frac{\mathrm{d}H}{\mathrm{d}T} v_i \Phi_j \mathrm{d}\Omega & \mathbf{x}_i \notin \Gamma_1 \\ 0 & \text{otherwise} \end{cases} \tag{27}$$

Finding apparent capacity dH/dT directly from enthalpy-temperature relation is not desirable as there is a possibility of oscillations due to its step-like behavior (Dalhuijsen and Segal, 1986). There are many approximate techniques which are proposed in literature [Morgan, Lewis and Zienkiwich (1978); Giudice, Comini and Lewis (1978); Lemmon (1981)] with reference to finite element method. Among these, the approach proposed by Lemmon (1981) is very popular. This approximation is expressed as

$$\frac{\mathrm{d}H}{\mathrm{d}T} = \sqrt{\frac{\left(\frac{\partial H}{\partial x}\right)^2 + \left(\frac{\partial H}{\partial y}\right)^2}{\left(\frac{\partial T}{\partial x}\right)^2 + \left(\frac{\partial T}{\partial y}\right)^2}} \tag{28}$$

3.4 Time-Stepping Algorithm

Spatial discretization of governing partial differential equation results in a system of semi-discrete ordinary differential equations given by Eq. (24), which still contains time derivative. A two level θ - method is used for time integration. It can vary between explicit and implicit strategies depending on the value of θ and results in the algebraic system

$$[\mathbf{C}(\mathbf{T}) + \theta\Delta t\mathbf{K}(\mathbf{T})]\mathbf{T}^{n+1} = [\mathbf{C}(\mathbf{T}) + (\theta - 1)\Delta t\mathbf{K}(\mathbf{T})]\mathbf{T}^n + \Delta t\mathbf{F}(\mathbf{T}) \tag{29}$$

where Δt is the time step and n denotes the time level (i.e.t_n= $n\Delta t$ if uniform time step is employed).

3.5 Solution of Non-Linear System

Equation (30) represents a system of nonlinear equations due to temperature dependent material properties. For such nonlinear problems, an iterative solution procedure is required. A *predictor-corrector* scheme based on direct substitution iteration (Lewis and Roberts, 1987) has been applied in the current analysis which has the following form:

Predictor step:

$$[\mathbf{C}(\mathbf{T}^n)+\theta\Delta t\mathbf{K}(\mathbf{T}^n)]\mathbf{T}_*^{n+1}=[\mathbf{C}(\mathbf{T}^n)+(\theta-1)\Delta t\mathbf{K}(\mathbf{T}^n)]\mathbf{T}^n+\Delta t\mathbf{F}(\mathbf{T}^n) \tag{30}$$

Corrector step:

$$[\mathbf{C}(\mathbf{T}^{\bar{n}})+\theta\Delta t\mathbf{K}(\mathbf{T}^{\bar{n}})]\mathbf{T}_{p+1}^{n+1}=[\mathbf{C}(\mathbf{T}^{\bar{n}})+(\theta-1)\Delta t\mathbf{K}(\mathbf{T}^{\bar{n}})]\mathbf{T}^n+\Delta t\mathbf{F}(\mathbf{T}^{\bar{n}}) \tag{31}$$

Predictor step computes temperature dependent terms using temperature of previous time level and predicts the nodal solution$\mathbf{T}_*^{n+1}$. Corrector step operates in a loop. All temperature dependent terms in the corrector step are evaluated at temperature $\mathbf{T}^{\bar{n}}$ which is given by

$$\mathbf{T}^{\bar{n}}=\gamma\mathbf{T}_p^{n+1}+(1-\gamma)\mathbf{T}^n,\quad \gamma\in(0,1) \tag{32}$$

where $\mathbf{T}_0^{n+1}=\mathbf{T}_*^{n+1}$ and p= 0,1,2,.... is the iteration counter. The loop of the corrector step terminates after achieving desired accuracy in results of successive stages at any time step. With this scheme, the time step is controlled by the number of iterations required to reach the state when $\left[\left\|\mathbf{T}_{p+1}^{n+1}-\mathbf{T}_p^{n+1}\right\| <\in\right]$ for some p and a user specified tolerance$\in$. If the number of iterations required becomes excessive, then the time step Δt is reduced. If very few iterations are needed for convergence, Δt may be increased.

For steady state problems, the above predictor-corrector scheme can be modified as:

Predictor step:

$$\mathbf{K}(\mathbf{T}_0)\mathbf{T}_*=\mathbf{F}(\mathbf{T}_0) \tag{33}$$

Corrector step:

$$\mathbf{K}(\mathbf{T}_{\bar{p}})\mathbf{T}_{p+1}^{=}\mathbf{F}(\mathbf{T}_{\bar{p}}) \tag{34}$$

where $\mathbf{T}_0$ is the initial guess, $\mathbf{T}_{\bar{p}}=\gamma\mathbf{T}_p+(1-\gamma)\mathbf{T}_{p-1}$, $\mathbf{T}_1=\mathbf{T}_*$ and p= 1,2,.... is the iteration counter.

4 Result and Discussions

We consider different irregular domains to perform nonlinear heat conduction analysis. Initially, problems without phase change are analyzed. Thermo- physical properties of the material depend on temperature. Linear as well as quadratic bases are used for MLS approximation of trial function. Problems are also solved using

FEM with ANSYS 9.0. Quadratic triangular elements have been used in finite element analysis. Same nodal arrangement is imported to perform MLPG analysis. Circle has been chosen as local quadrature domain in MLPG analysis. Radius of the quadrature domain, r_Q has been calculated by the formula [Liu (2003)]

$$r_Q = \alpha_Q d_c \tag{35}$$

where α_Q is dimensionless size of the corresponding domain and d_c is the characteristic length between any node and its neighbors. Radius of local domain near the global boundary is modified if required to avoid intersection with global boundary. Radius of the support domain,r_S is calculated using the method used by Sterk and Trobec (2008). 12-15 nodes in support domain in case of linear basis and 15-18 nodes in case of quadratic basis are found to provide accurate results. Dimensionless size of local domain α_Q varies between 0.7-0.9 to yield results closer to that of FEM. The θ - *method* is used to perform the temporal discretization (with θ =1) and iterative *predictor-corrector* scheme has been applied to take care of the nonlinearity of the problem [Thakur, Singh and Sahoo (2009)]. All the required codes have been developed in C++. Experiments are carried out with different number of nodes in the support domain and different values of α_Q to vary the size of local domain. Finally, parameters are selected to minimize the error.

4.1 Test Problem 1: Arc Shaped Domain

Let us consider an arc shaped irregular domain shown in Fig. 1. Circular segment ABCD is a part of a circle of radius R centered at O. Height H of the arc is less than R. Neither Cartesian coordinate system nor cylindrical system can naturally map the geometry. Temperature of the bottom base is T_B and of the curved top is T_T. All the parameters used for the analysis are listed in Tab. 1. Experiments are performed with 37, 61, 91 and 331 field nodes in transient and steady state conditions. Nodal arrangements are shown in Fig. 2. Method of direct interpolation provides linear equation at each essential boundary node using the shape functions created on that node. Hence, local domains around boundary nodes are not required. Figure 3 depicts the discretization of the problem domain with 37 nodes, local domains of all the internal nodes and distribution of Gauss points for numerical integration. Steady state analysis has been carried out at using linear and quadratic basis for the function approximation. Results of FEM and MLPG method are drawn together to compare the results.

Figure 4 shows the temperature variation across the plane of symmetry of the computational domain. Temperature distribution in the entire domain is shown in Fig. 5. These plots have been drawn for the results obtained with 331 field nodes in the computational domain. Twelve field nodes in support domain in case of linear

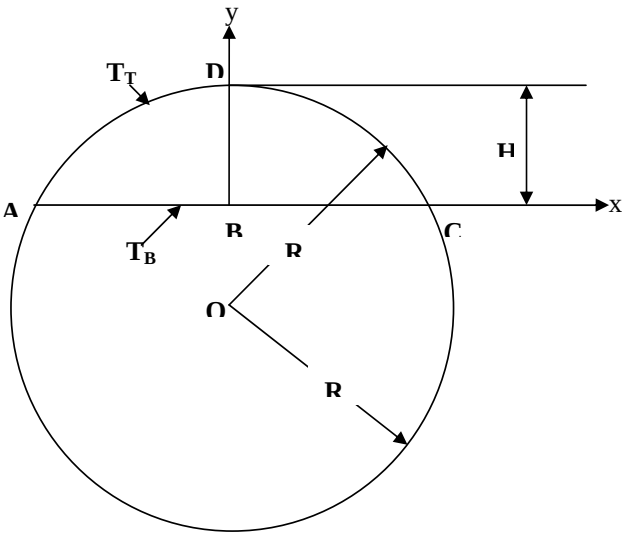

Figure 1: Problem definition of arc shaped problem domain (ABCD)

Table 1: Data for arc shaped problem

Parameter	Value of the parameter
Radius of the arc (R)	1 m
Height of the arc (H)	0.5m
Density (ρ)	$\rho = \rho_0$(1- 0.000001T) where ρ_0 =9000 kg/m^3
Specific heat (c)	$c(T) = c_0$ (1 + 0.0001T) where c_0 = 400 J/kg °C
Thermal conductivity (k)	$k(T) = k_0$(1+ 0.0001T) where k_0 = 400W/m °C
Uniform heat generation (Q_g)	0W/m^3
Base temperature(EBC1), T_B	200 °C
Curved top temperature(EBC2), T_T	100 °C
Initial Temperature	100 °C
Time step size(Δt)	50 s

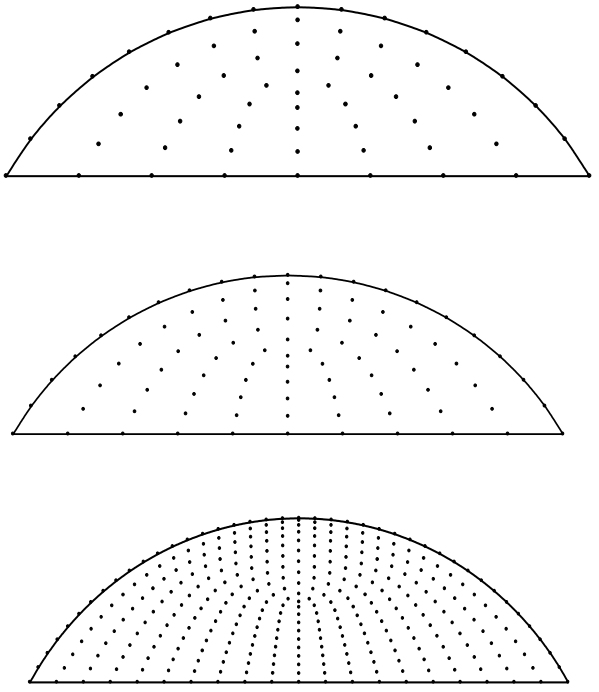

Figure 2: Arc shaped computational domain with 61, 91 and 331 field nodes

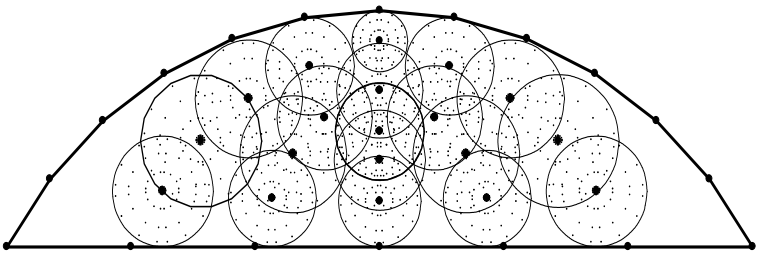

Figure 3: Domain with 37 nodes, local domains of all internal nodes and distribution of Gauss points

basis and fifteen field nodes in the support domain in case of quadratic basis have been taken for the analysis. Plots confirm a good agreement of MLPG results with that of FEM. Results of MLPG method with quadratic basis are closer to FEM than these of linear basis. Relative error based on L_2 norm has also been listed in Tab. 2 against the number of nodes used for steady state analysis. FEM results are used as the base result for the calculation of relative error. These data also confirm better results with quadratic basis and good convergence of MLPG method.

Transient analysis of the same model problem has also been carried out. Results are compared with the results of FEM. A typical isotherm progress has been drawn in Fig. 6 at different levels of time. These plots show a good agreement between the results of FEM and MLPG method. It is observed that isotherms move at faster rate at the initial period of time compared to same time interval later. Temperature-time history of a typical point drawn in Fig. 7 shows that the nature of temperature rise captured by MLPG is quite close to that of FEM. Temperature of a point, close to the essential boundary of lower temperature value of the computational domain, increases rapidly and finally becomes constant, indicating attainment of steady state.

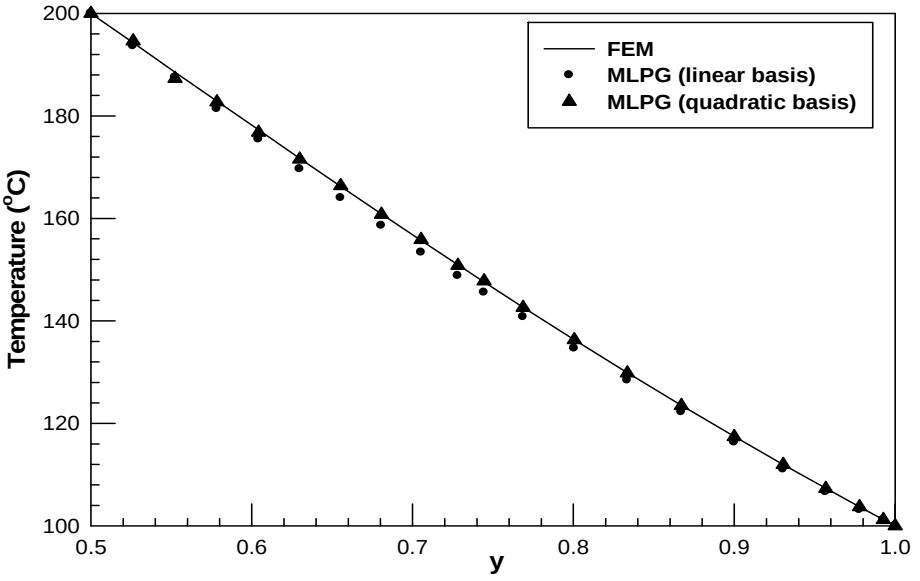

Figure 4: Temperature variation along the line of symmetry

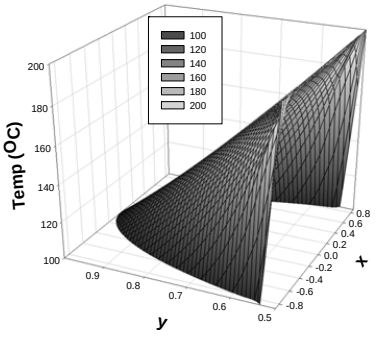

a. FEM

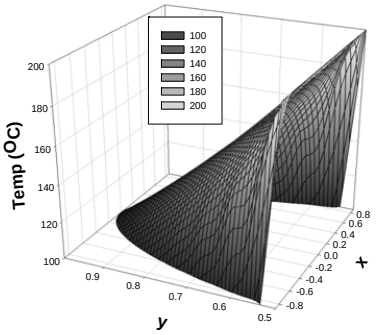

b. MLPG(linear basis)

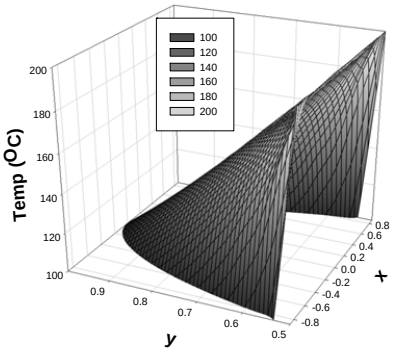

c. MLPG (quadratic basis)

Figure 5: Temperature variation for steady state condition for the arc shaped domain

Table 2: Relative error based on L_2 norm with number of nodes

Number of nodes	**Relative Error**	
	MLPG (linear basis)	**MLPG (quadratic basis)**
37	0.0211	0.0108
61	0.0171	0.0088
91	0.0144	0.0088
331	0.0119	0.0033

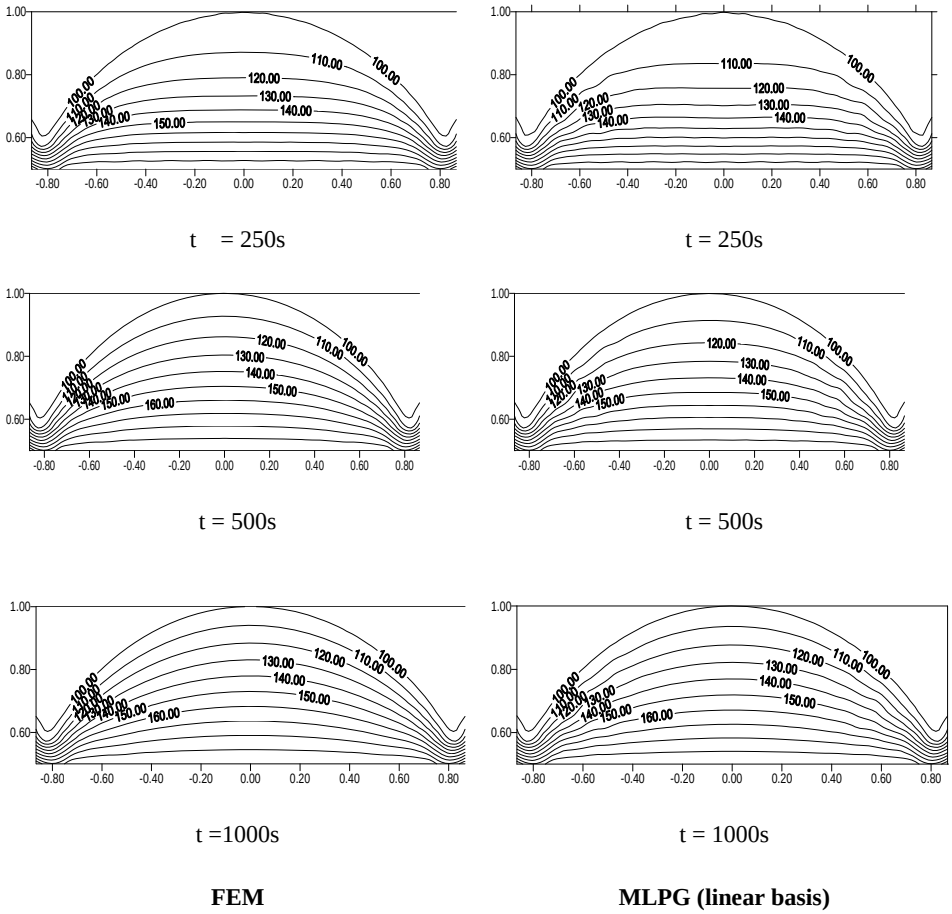

Figure 6: Isotherm progress for the transient problem of the arc shaped domain

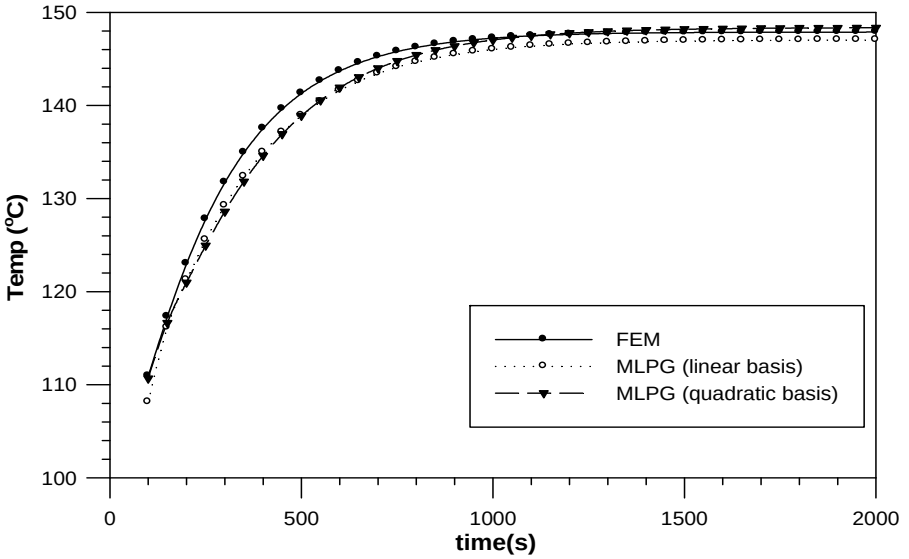

Figure 7: Temperature-time history of point (0, 0.7449) in case of the arc shaped Domain

4.2 Test Problem 2: Square Domain with an Eccentric Hole

Second irregular domain is a square having a hole at any arbitrary eccentric location. In this domain, surface of the circular hole is maintained at a fixed temperature and all the sides of the square are exposed to convective environment. In the previous example of irregular domain, only essential boundary conditions were considered which made formulation easier as local domains on the boundary nodes were not required. This example involves different types of boundary conditions along with the variation in the properties of the material. Domain has been analyzed with 129, 241 and 481 nodes. One of such nodal arrangements is shown in Fig. 8.

Ten Gauss points have been used in each boundary edge of the local domain along the boundary of the problem domain. Gauss points inside the local domain are arranged similarly as shown in Fig. 8. All the required parameters for the analysis of the problem are listed in Tab. 3. All the thermo-physical properties of the material are dependent on the temperature. Radius of local domain varies as the nodal density is different in the different parts of the computational domain. Radius of local domain for nodes near boundary is modified so that formation of irregular local domains on the global boundary can be avoided as performing numerical integration

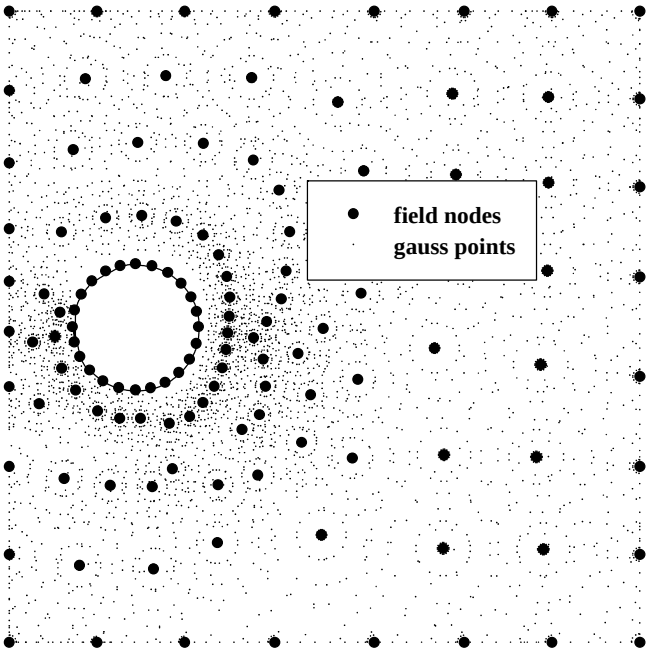

Figure 8: Computational domain with 129 field nodes and all Gauss points

in such domains is computationally expensive.

Variation of radius of local domains in the entire domain is drawn in Fig. 9. As nodal density is very high near the boundary of the hole, the local domain radius attains a minimum in this region. Local domains created on the corners of square domain are the quadrants of a circle and on the sides of the square are semicircles, which can be easily transformed into the standard square.

Results of steady state analysis are shown in Fig. 10. These plots are drawn for a 129 irregular field nodes in the computational domain. FEM results are obtained for the same nodal arrangement with ANSYS 9.0. Linear as well as quadratic bases have been used in MLS formulation. Result of MLPG formulations with linear and quadratic basis are quite similar to the one obtained by FEM. However, it is observed that results of MLPG method with quadratic basis are closer to FEM results than the results with linear basis.

Transient analysis of the problem has also been carried out. Results obtained by MLPG method are found to be in good agreement with the results of FEM. Temperature-time history of a set of points from different region has been captured and drawn in Fig. 11. Temperature rise patterns of the corners of the squares are shown in Fig. 11 (a) and 11 (b) and they are different in nature. This is because of eccentric location of the hole in the computational domain. The point selected in Fig. 11 (a) is closer to the hole which is maintained at higher temperature, the rise in temperature starts earlier as compared to the point selected in Fig. 11 (b). As the point for Fig. 11 (d) is the closest to the hole, very high rate of temperature rise at this point can be seen.

Table 3: Data for sample problem 2: Square with eccentric hole

Parameter	Value of the parameter
Side of square	1 m
Radius of hole	0.1 m
Center of the hole	(0.2m, 0.5m)
Density (ρ)	$\rho = \rho_0$(1- 0.000001T) where ρ_0 =9000 kg/m^3
Specific heat (c)	$c(T) = c_0\ (1 + 0.0001T)$ where c_0 = 400 J/kg °C
Thermal conductivity (k)	$k(T) = k_0$(1+ 0.0001T) where k_0 = 400W/m °C
Uniform heat generation (Q_g)	0W/m^3
Temperature of the surface of circular hole (EBC)	200 °C
Ambient temperature, T_a	30 °C
Convection coefficient, h	10 kW/m^{2o}C
Initial Temperature	100 °C
Time step size(Δt)	50 s

4.3 Test Problem 3: One-dimensional Phase Change Problem

Test problems 3 and 4 analyse phase change problems. Apparent capacity method is used to solve the governing differential equation together in solid and liquid phases. Lemmon's approximation technique [Lemmon (1981)] is used to calculate apparent capacity.

Test problem 3 is a one-dimensional problem which is originally solved by Voller (1987). This problem has been picked up to verify the MLPG result. The initial temperature of the phase change material is assumed to be above solidification temperature. Relevant data associated with the problem are listed in the Tab. 4.

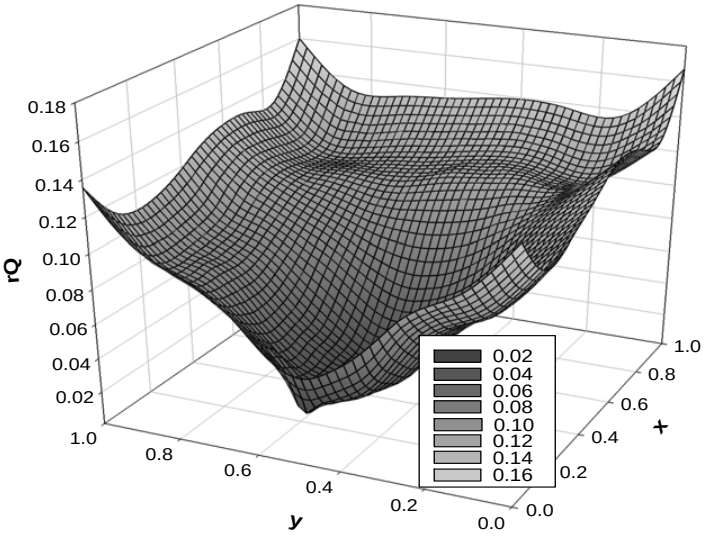

Figure 9: Variation of local domain radius in the square domain with eccentric hole

Table 4: Data for 1-D phase change problem

Parameter	Value of the parameter
Length (L)	1 m
Density (ρ)	1 kg/m^3
Specific heat (c)	25×10^6 J/kg °C
Thermal conductivity (k)	2 W/m °C
Latent heat (L)	10^8J/kg
Phase change temperature, T_f	0°C
Phase change interval, $(T_{f1}-T_{f2})$	1°C
Left end temperature(EBC1), T_L	-10°C
Right end temperature(EBC2), T_R	2°C
Initial Temperature, T_o	2°C
Time step size(Δt)	3600 s

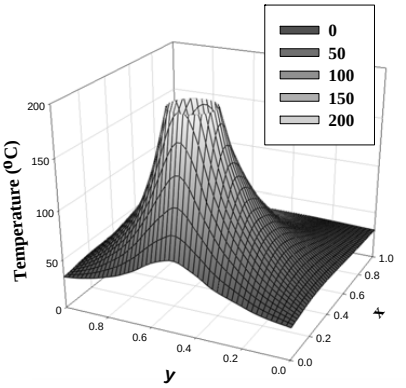

(a) FEM

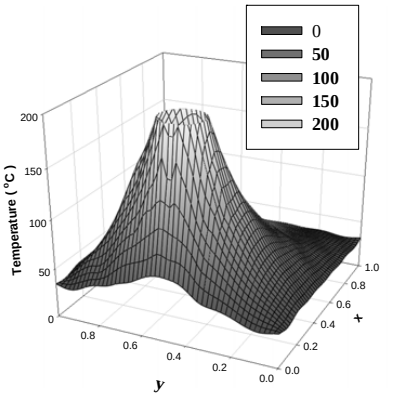

(b) MLPG with linear basis

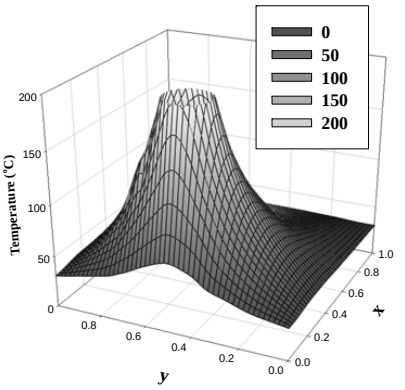

(c) MLPG with quadratic basis

Figure 10: Temperature variation in steady state condition in the square domain with eccentric hole

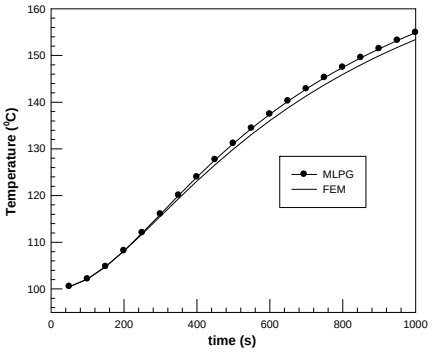

(a) for point (0,1)

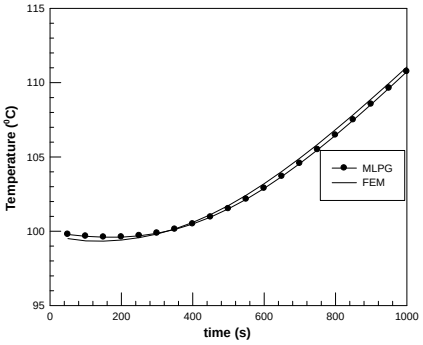

(b) for point (1,1)

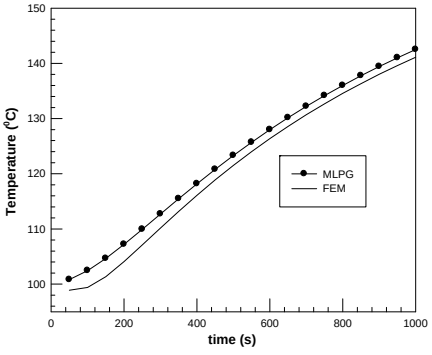

(c) for point (0.38, 0.89)

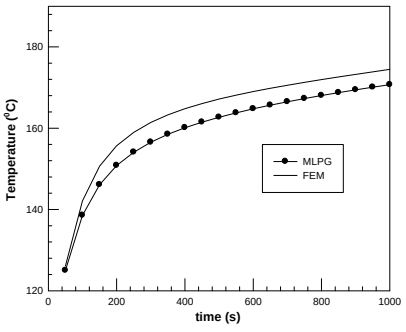

(d) for point (0.38, 0.48)

Figure 11: Temperature-time history of some typical points in the square domain with eccentric hole

Solidification front movement obtained by the MLPG method is very close to the analytical solution of the problem as shown in Fig. 12. Temperature variation shown in Fig. 13 also depicts the movement of interface with time. Temperature varies more rapidly in the solid region as compared to the liquid region (Fig. 13) which indicates higher rate of heat transfer through the solidified region. This satisfies the energy conservation at the interface, i.e. heat transfer through the solid is the summation of heat transfer rate through the liquid and rate of heat transfer needed for phase change at the solidification front.

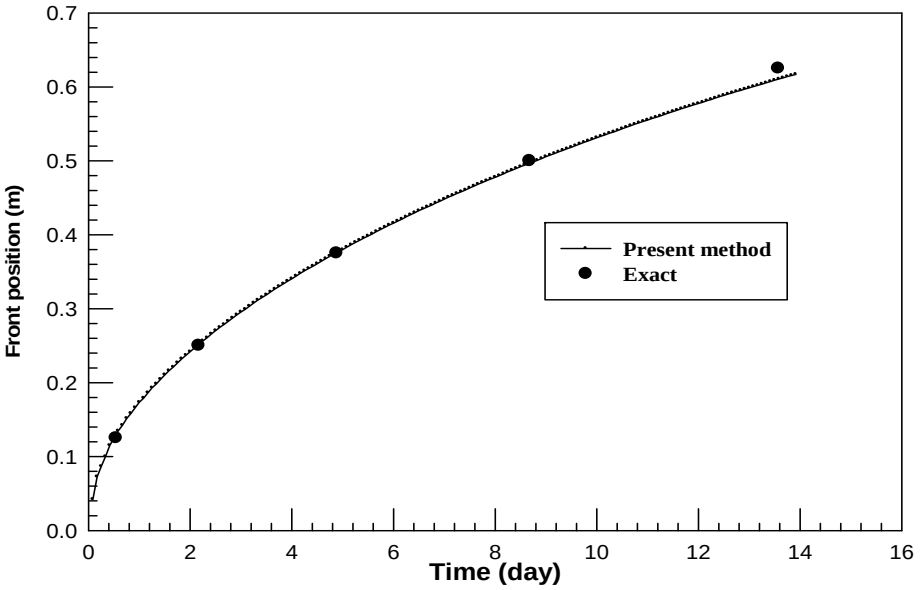

Figure 12: Phase front movement during the solidification of semi-infinite slab of iquid (51 field nodes, T_o= 2°C, T_f= 0°C, T_w=-10°C and L = 100 MJ/kg)

4.4 Test Problem 4: Square with an Eccentric Hole

Let us consider domain of test problem 2 for phase change analysis. Relevant data of the problem are listed in the Tab. 5. Thermo-physical properties of the material correspond to paraffin RT 60 used in solar energy storage [Velraj, Seeniraj, Hafner, Faber, and Schwarzer (1997)]. This is computationally more challenging problem which has been solved using MLPG method. Sides of the square are exposed to convective boundary condition while the surface of eccentric hole remains at a temperature below T_f. Problem has been defined in Fig. 14. Initial temperature of the liquid is higher than the freezing temperature. One of the typical arrangements of field nodes and corresponding Gauss points are shown in 8. Isotherms in the solid region at different times during the evolution are shown in Fig. 15. Interface coincides with the isotherm of 58°C. Solidification starts around the hole and progresses in the liquid.

Sides of the square also lose heat by convection. As a result, corners solidify earlier, and solidification finishes somewhere between the hole and the farthest side from the hole. Temperature-time history of different points is depicted in Fig. 16.

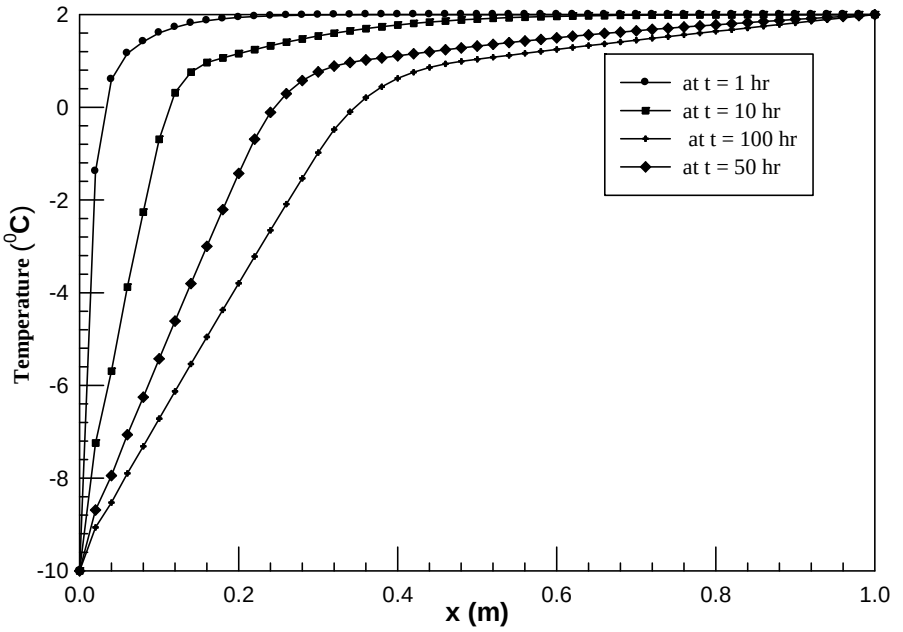

Figure 13: Variation of temperature in the domain at different level of time

Table 5: Data for 2-D irregular domain (square with an eccentric hole)

Parameter	Value of the parameter
Dimensions of square ($L \times B$)	1 m $\times$ 1 m
Radius of the central hole, r_i	0.1 m
Density (ρ)	800 kg/m^3
Specific heat (c)	900 J/kg °C
Thermal conductivity (k)	0.2 W/m °C
Latent heat (L)	214 kJ/kg
Temperature of the surface of hole (EBC), T_W	56°C
Phase change temperature (T_f)	59°C
Phase change interval, ($T_{f1} - T_{f2}$)	2°C
Initial Temperature, T_o	61°C
Time step size(Δt)	1000 s

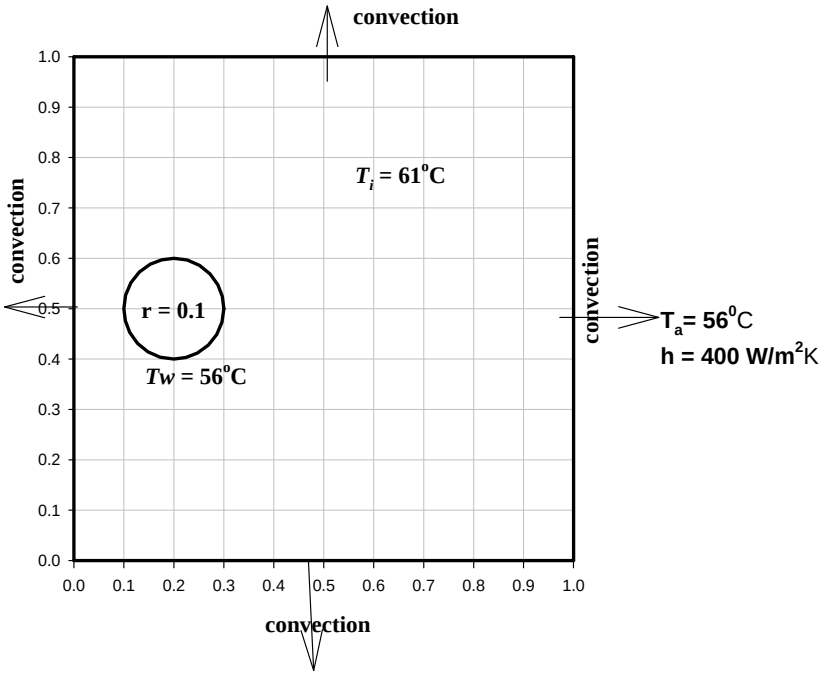

Figure 14: Square domain with an eccentric hole: geometry, initial and boundary Conditions

Locations of the selected points are shown in the center. Plots are excellent representation of phase change phenomena. Points shown in Fig. 16 (a) and (b) are near the center of the domain, hence interface reaches there after some time from when it starts. Due to cumulative effects of convection and point being closer to the hole, temperature decreases very fast at the point shown in Fig. 16 (c). Point (d) is near the corner (1, 1). The convection effect is dominant but as the point is farther from the hole than the previous one, difference can be seen in the temperature-time history of the point.

4.5 Test Problem 5: Continuously Nonhomoneous Functionally Graded Material (FGM)

Heat conduction in a functionally graded material is solved using MLPG method in this section. Codes developed for homogeneous nonlinear conduction problems are extended to solve the nonhomogeneous test problem with some modifications. The governing differential equation of heat conduction in continuously nonhomo-

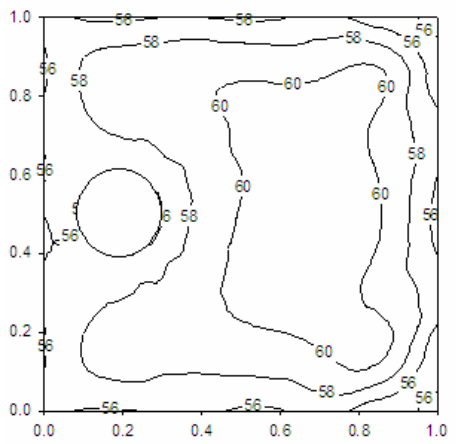

(a) at t = 10000 s

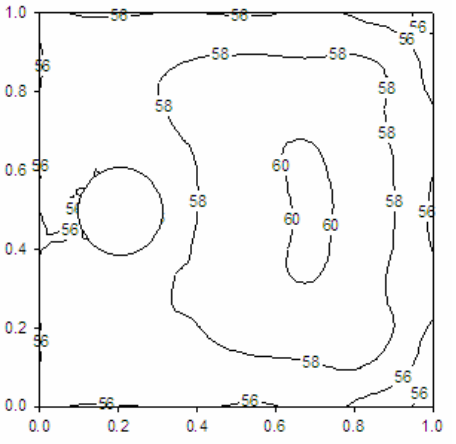

(b) at t = 20000 s

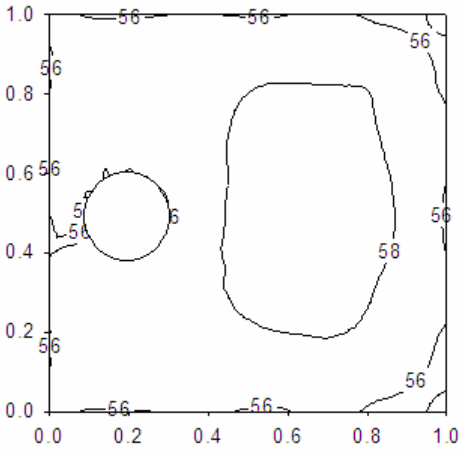

(c) at t = 30000 s

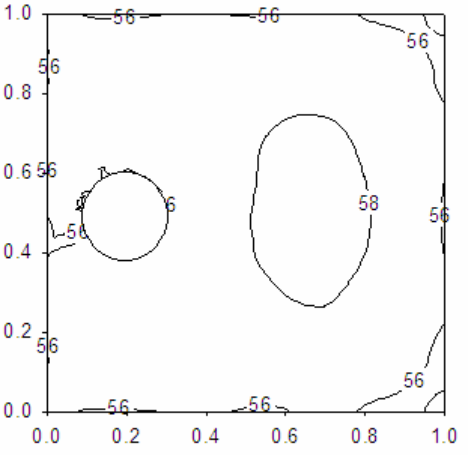

(d) at t = 40000 s

Figure 15: Phase front (58°C isotherm) progress during freezing of liquid in a long square duct with an eccentric hole (129 field nodes, T_o= 61°C, T_f= 59°C, T_w= 56°C and L = 214 kJ/kg)

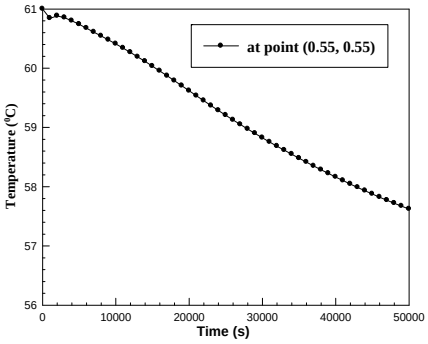

(a)

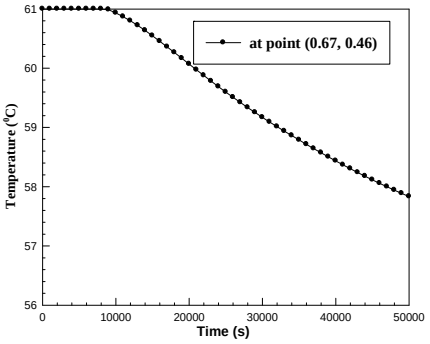

(b)

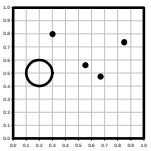

Domain and location of selected field nodes

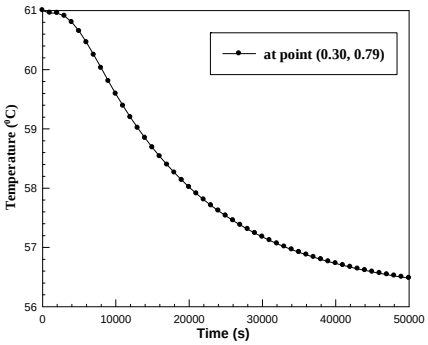

(c)

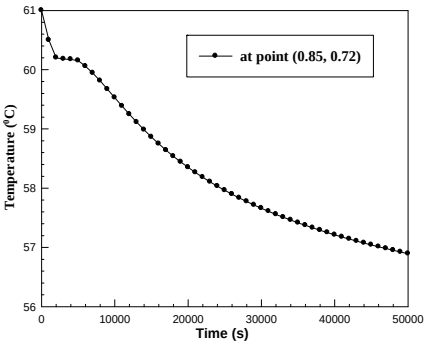

(d)

Figure 16: Temperature–time history of a few typical field nodes

geneous medium is given by

$$\nabla \cdot [k(\mathbf{x})\nabla T] + Q_g(\mathbf{x}) = \rho(\mathbf{x})c(\mathbf{x})\dot{T} \tag{36}$$

MLPG formulation of the problem with similar boundary conditions shown in Eq. (2) and Eq. (3) yields conventional matrix form given by

$$\mathbf{C}\dot{\mathbf{T}} + \mathbf{K}\mathbf{T} = \mathbf{F} \tag{37}$$

where matrices are **C**, **K** and **F** are as follows:

$$C_{ij} = \begin{cases} \int\limits_{\Omega_Q} \frac{\rho(\mathbf{x})c(\mathbf{x})}{k(\mathbf{x})} v_i \Phi_j \mathrm{d}\Omega & \mathbf{x}_i \notin \Gamma \\ 0 & \text{otherwise} \end{cases} \tag{38}$$

$$K_{ij} = \begin{cases} \Phi_j & \mathbf{x}_i \in \Gamma_1 \\ \left[\int\limits_{\Omega_Q} \nabla v_i . \nabla \Phi_j \mathrm{d}\Omega - \int\limits_{\Omega_Q} \frac{1}{k(\mathbf{x}_j)} (\nabla k . \nabla \Phi_j) \mathrm{d}\Omega - \int\limits_{\Gamma_{1Q}} \frac{v_i}{k(\mathbf{x}_j)} \frac{\partial \Phi_j}{\partial n} \mathrm{d}\Gamma + \int\limits_{\Gamma_{3Q}} \frac{h}{k(\mathbf{x}_j)} v_i \Phi_j \mathrm{d}\Gamma \right] & \\ & \mathbf{x}_i \notin \Gamma_1 \end{cases} \tag{39}$$

$$F_i = \begin{cases} \bar{T} & \mathbf{x}_i \in \Gamma_1 \\ \int\limits_{\Gamma_{2Q}} \frac{\bar{q}}{k(\mathbf{x}_j)} v_i \mathrm{d}\Gamma + \int\limits_{\Gamma_{3Q}} v_i \frac{h}{k(\mathbf{x}_j)} T_a \mathrm{d}\Gamma + \int\limits_{\Omega_Q} \frac{Q_g}{k(\mathbf{x}_j)} v_i \mathrm{d}\Omega & \text{otherwise} \end{cases} \tag{40}$$

where $\Gamma_{1Q} = \Gamma_1 \cap \partial\Omega_Q$, $\Gamma_{2Q} = \Gamma_2 \cap \partial\Omega_Q$ and $\Gamma_{3Q} = \Gamma_3 \cap \partial\Omega_Q$.

A test problem of finite strip as solved by Sladek et al. (2003) has been chosen for analysis. Thermal conductivity of the material varies exponentially in space, so does the thermal diffusivity. This variation can be expressed as

$$k(\mathbf{x}) = k_0 e^{\gamma x} \tag{41}$$

The parameters used in one-dimensional analysis of the test problem are listed in Tab. 6. The computational domain with 21 field nodes is shown in Fig. 17.

Analytical solution of the this problem is given by

$$T(x) = T_R \frac{e^{-\gamma x} - 1}{e^{-\gamma l} - 1} \tag{42}$$

MLPG results at some typical locations in steady state condition are presented in Tab. 7 along with corresponding exact solution. Results are found to be very close

Table 6: Data for non-homogeneous problem

Parameter	Value of the parameter
Length of the domain (l)	0.04 m
Density (ρ)	1000 kg/m^3
Specific heat (c)	1000 J/kg °C
Thermal conductivity (k)	$k(\mathbf{x}) = k_0 e^{\gamma x}$where k_0 = 17 W/m °C
Uniform heat generation (Q_g)	0W/m^3
Left boundary temperature (EBC1), T_L	0 °C
Right boundary temperature (EBC2), T_R	1 °C
Initial Temperature, T_i	0 °C
Gama (used in $k(\mathbf{x}) = k_0 e^{\gamma x}$)	0 m^{-1}, 20 m^{-1}, 50 m^{-1}
Time step size(Δt)	1 s

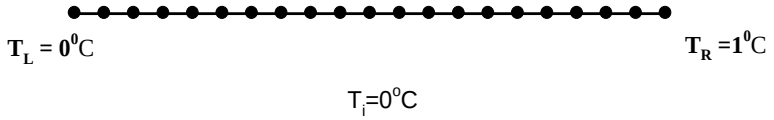

Figure 17: Computational domain with 21 field nodes

with each other. Codes are further verified in case of transient analysis by matching MLPG results with corresponding exact solution available for homogeneous medium ($\gamma = 0$). Variations of temperature in the computational domain at different time level are shown in Fig. 18. MLPG results agree well with the exact solutions. Finally, variation of temperature at x/l=0.25 is shown in Fig. 19 for different values of gama. Results are found to be in good agreement with the results obtained by Sladek et al. (2003).

5 Conclusion

The MLPG method, due to its flexibility in formulation, is found suitable to apply on the problems of nonlinear heat conduction. Performing integration in local domain within the computational domain has removed the need of global mesh which alleviates the problem of remeshing associated with FEM. Careful selection of dimensions of different domains of MLPG yields very accurate results. Iterative predictor-corrector method handles issues of nonlinearity very well. Apparent capacity method with Lemmon's approximation technique is found working well

Table 7: Comparison of MLPG results with exact solution at some typical locations in steady state condition

Location (x/l)	**Temperature (°C)**			
	$\gamma = 20\text{m}^{-1}$		$\gamma = 50\text{m}^{-1}$	
	MLPG	Exact	MLPG	Exact
0.2	0.274	0.268	0.388	0.381
0.3	0.391	0.387	0.526	0.521
0.4	0.500	0.497	0.641	0.636
0.5	0.601	0.598	0.733	0.731
0.6	0.693	0.692	0.809	0.808
0.7	0.779	0.778	0.871	0.871
0.8	0.858	0.858	0.922	0.923
0.9	0.931	0.932	0.964	0.965

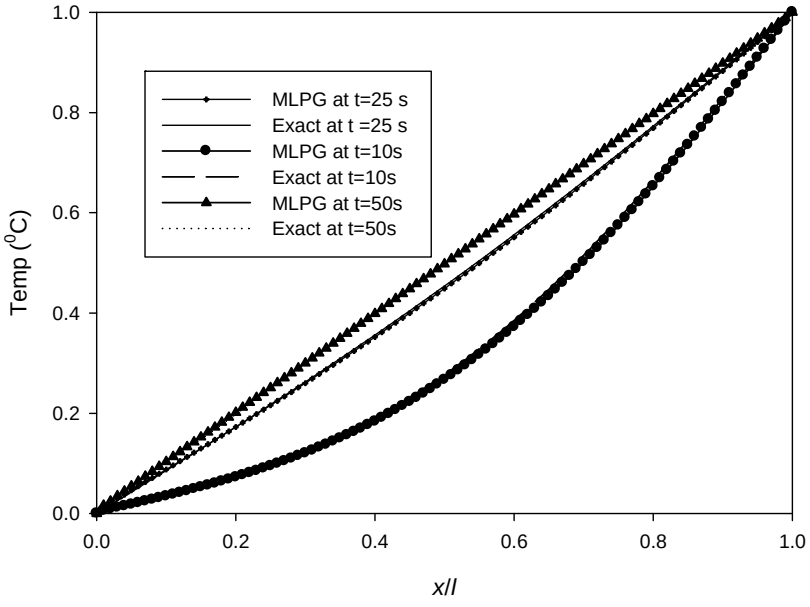

Figure 18: Variation of temperature in the computational domain at different time levels for homogeneous material (gamma = 0)

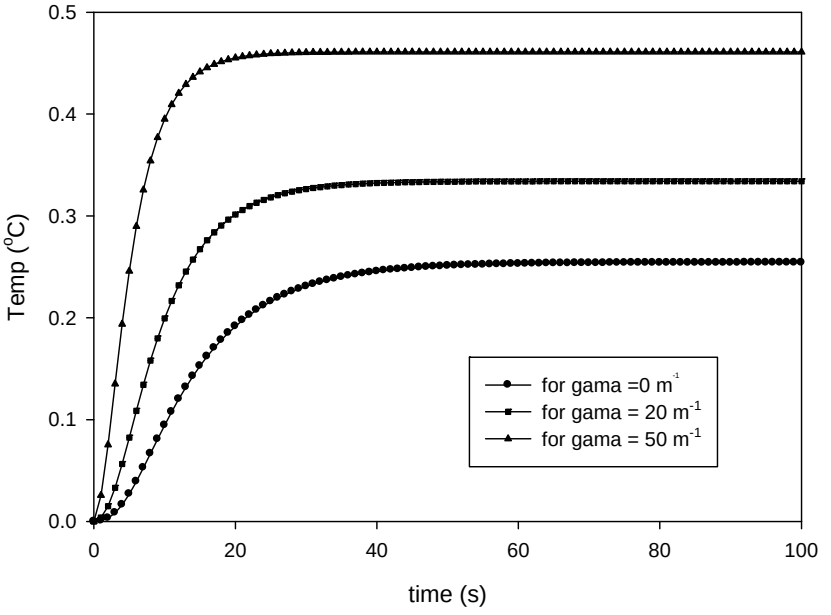

Figure 19: Variation of temperature at $x/l = 0.25$

with MLPG method. Finally, it can be concluded that the MLPG method is a very good choice to solve the problems of homogeneous as well as non-homogeneous nonlinear heat conduction in irregular domains including problems of phase change without meshing and remeshing of computational domain.

References

Atluri, S. N.; Zhu,T. (1998a): A new meshless local Petrov–Galerkin (MLPG) approach in computational mechanics, *Comput. Mech.*, vol. 22, pp. 117-127.

Atluri, S. N.; Zhu,T. (1998b): A new meshless local Petrov–Galerkin (MLPG) approach to nonlinear problems in computational modeling and simulation, *Comput. Modeling Simulation Eng.*, vol. 3, pp. 187–196.

Atluri, S. N.; Zhu,T. (2000): The meshless local Petrov-Galerkin approach for solving problems in elasostatics, *Comput. Mech.*, vol. 25, pp. 169-179.

Atluri, S. N.; Shen, S. (2002a): The meshless local Petrov–Galerkin (MLPG) method: A simple and less costly alternative to the finite element and boundary

element methods, *CMES: Computer Modeling in Engineering & Sciences*, vol. 3, pp. 11–52.

Atluri, S. N.; Shen, S. (2002b): *The Meshless Local Petrov-Galerkin Method,* Tech Science Press, Los Angeles.

Babuska, I.; Melenk, J. M. (1997). The Partition of Unity Method. *Int. J. Numer. Methods Eng.*, vol. 40, pp. 727-758.

Bathe, K. J.; Koshgoftaar, M. R. (1979): Finite element formulation and solution of nonlinear heat transfer, Nuclear. *Eng. Des.* vol. 30, pp. 205-213.

Chan, C. L. (1993): A local iteration scheme for nonlinear two-dimensional steady state heat conduction: A BEM approach, *Appl. Math. Modell.,* vol.17, pp. 650-657.

Dalhuijsen, A. J.; Segal, A. (1986). Comparison of finite element techniques for solidification problems. *Int. J. Numer. Methods Eng.*, vol. 23, pp. 1807-1829.

Del Giudice, S.; Comini, G.; Lewis, R.W. (1978). Finite element simulation of freezing processes in soils, *Int. J. Numer. Anal. Methods Geomech.*, vol. 2, pp. 223-235.

Lancaster, P.; Salkauskas, K. (1981): Surfaces generated by moving least squares methods. *Math. Comput.*, vol. 37, pp. 141-158.

Lemmon, E. G. (1979): Phase change techniques for finite element codes, in Lewis, R. W. and Morgan, K. (eds), Numerical Methods in Thermal Problems (Proc. Conf.), Pineridge Press, Swansea, 149-158.

Liao, S. (1997): General boundary element method for non-linear heat transfer problems governed by hyperbolic heat conduction equation, *Comput. Mech.*, vol. 20, pp. 397-406.

Ling, C. S.; Surana, K. S. (1994): p-Version finite element formulation for axisymmetric heat conduction with temperature dependent thermal conductivities, *Comput. Struct.,* vol. 52, pp. 353-364.

Liu, G. R. (2002): *Meshfree Method: Moving beyond the finite element method,* CRC Press, BOCA Raton, FL.

Liu, K.Y.; Long, S.Y.; Li, G.Y. (2008): A Meshless Local Petrov-Galerkin Method for the Analysis of Cracks in the Isotropic Functionally Graded Material, *CMC: Computers, Materials, & Continua*, Vol. 7, No. 1, pp. 43-58.

Liu, W. K.; Chen, Y; Chang, C. T.; and Belytschko, T. (1996). Advances in multiple scale kernel particle methods. *Comput. Mech.*, vol. 18, pp. 73-111.

Morgan, K.; Lewis, R. W.; Zienkiwicz, O. C. (1978). An improved algorithm for heat conduction problems with phase change, *Int. J. Numer. Methods Eng.*, vol. 12, pp. 1191-1195.

Quin, L. F.; Batra, R. C. (2005): Three dimensional transient heat conduction in a functionally graded thick plate with higher order plate theory and a meshless local Petrov-Galerkin method, *Comput. Mech.*, vol. 32, pp. 214-226.

Shepard, D. (1968): A two-dimensional function for irregularly spaced points. Proc. of ACM National Conference, pp. 517-524.

Singh, A.; Singh, I. V.; Prakash, R. (2006): Numerical solution of temperature-dependent thermal conductivity problems using a meshless method, *Numer. Heat Transfer B,* vol. 50, pp. 125-145.

Singh, A.; Singh, I. V.; Prakash, R. (2007): Meshless element free Galerkin method for unsteady nonlinear heat transfer problems, *Int. J. of Heat Mass Transfer,* vol. 50, pp. 1212-1219.

Sladek, J.; Sladek, V.; Atluri, S. N. (2004): Meshless local Petrov-Galerkin method for heat conduction problem in an anisotropic medium, *CMES: Computer Modeling in Engineering & Sciences*, vol. 6, pp. 309-318.

Sladek, J.; Sladek, V.; Zhang, Ch. (2003): Transient heat conduction analysis in functionally graded materials by the meshless loca boundary integral equation method, *Computational Material Science*, vol. 28, pp. 494-504.

Sterk, M.; Trobec, R. (2008): Meshless solution of a diffusion equation with parameter optimization and error analysis, *Eng. Anal. Boundary Elem.,* vol. 32, pp. 567-577.

Thakur, H. C.; Singh, K. M.; Sahoo, P. K. (2009): Meshless Local Petrov-Galerkin Method for Nonlinear Heat Conduction Problems, *Numer. Heat Transfer B*, Part B, vol. 56, pp. 393- 410, 2009.

Trujillo D. M.; Busby, H. R. (1977): Finite element nonlinear analysis using a stable explicit method, *Nuclear. Eng. Des.,* vol. 44, pp. 227-233.

Velraj, R.; Seeniraj, R. V.; Hafner, B.; Faber, C.; Schwarzer, K. (1997). Experimental analysis and numernical modeling of inward solidification of a finned vertical tube for a latent heat storage unit. *Sol. Energy*, vol, 60, pp. 281-290.

Voller, V. R. (1987). An implicit enthalpy solution for phase change problems: with application to binary alloy solidification. *Appl. Math. Modell.,* vol. 11, pp. 110-116.

Wendland, H. (1995). Piecewise polynomial, positive definite and compactly supported radial basis functions of minimal degree. *Journal of Approximate Theory*, vol. 93, pp. 258-272.

Wu, X.-H.; Tao, W.-Q. (2008): Meshless method based on the local weak-forms for steady-state heat conduction problems, *Int. J. of Heat Mass Transfer,* vol. 51, pp. 3103-3112.

Yang, H. (1999): A precise algorithm in the time domain to solve the problem of heat transfer, *Numer. Heat Transfer B,* vol. 35, pp. 243-249.